nature
structural &
molecular biology

Molecular determinants of gating at the potassium-channel selectivity filter

Julio F Cordero-Morales[1,3], Luis G Cuello[1,3], Yanxiang Zhao[2], Vishwanath Jogini[2,3], D Marien Cortes[1,3], Benoît Roux[2,3] & Eduardo Perozo[1,3]

We show that in the potassium channel KcsA, proton-dependent activation is followed by an inactivation process similar to C-type inactivation, and this process is suppressed by an E71A mutation in the pore helix. EPR spectroscopy demonstrates that the inner gate opens maximally at low pH regardless of the magnitude of the single-channel-open probability, implying that stationary gating originates mostly from rearrangements at the selectivity filter. Two E71A crystal structures obtained at 2.5 Å reveal large structural excursions of the selectivity filter during ion conduction and provide a glimpse of the range of conformations available to this region of the channel during gating. These data establish a mechanistic basis for the role of the selectivity filter during channel activation and inactivation.

The activity of ion channels is governed by mechanisms that allow the selective conduction of ions across the membrane and control the onset and duration of the conductive state (gating). At the single-channel level, gating is characterized by transitions between conductive and nonconductive conformations via structural rearrangements along the permeation path[1,2]. We have studied the prokaryotic K^+ channel KcsA[3] from *Streptomyces lividans* in an attempt to develop a mechanistic understanding of the molecular events that underlie gating in K^+ channels. KcsA is activated by protons[4] acting on the intracellular side of the channel[5]. Additionally, open probability (P_o) is modulated by transmembrane voltage, in spite of the absence of a canonical voltage sensor (refs. 4,5 and accompanying paper[6]). EPR spectroscopic experiments have shown that KcsA gating is associated with a movement of at least 9 Å at the base of the TM2 inner helix bundle[7–9]. This type of movement is related to the conformational changes described in voltage-dependent and inward-rectifier K^+ channels by indirect methods[10–13] and may correlate with the open conformations observed in the crystal structures of MthK and KvAP[14,15].

Even when maximally activated, KcsA opens with a very low P_o under steady-state conditions (from <0.03 to 0.2)[4,5,16]. If the EPR-determined movement of the inner helices indeed reflects the structural changes in the closed-to-open transition, why does KcsA have such a low P_o? We have suggested that this contradiction could be resolved if the low P_o were due to other structural elements in KcsA (for example, the selectivity filter) acting in concert with the opening of the inner helix bundle[7]. Several pieces of evidence point to the selectivity filter as a region with a great deal of influence over the gating behavior of K^+ channels, including the effect of certain permeant ions on gating[17–20], the effect of unnatural amino acid mutagenesis at the selectivity filter[21] and the role of subconducting states and specific P-loop mutants on single-channel gating kinetics[22–25]. Gating of K^+ channels at the level of the selectivity filter has traditionally been associated with C-type inactivation, a slow process by which the channel enters a nonconductive conformation and is sensitive to external K^+ concentration[26–29].

We have discovered a process that explains the low–open probability gating in KcsA through putative molecular rearrangements within the selectivity filter. This process seems to be related to C-type inactivation in voltage-gated (Kv) channels. Thus, this manuscript deals with two key issues regarding the molecular basis of inactivation gating in K^+ channels: defining the roles of different structural elements in stationary and nonstationary gating and establishing the structural basis that underlies gating at the selectivity filter.

RESULTS

An inactivation event during KcsA gating

To characterize the kinetic properties of pH-activated KcsA, we studied its single-channel behavior using liposome patch-clamp methods with purified preparations reconstituted at very low protein-to-lipid ratios. **Figure 1a** shows a representative 1-min section of a long single-channel recording obtained under symmetric K^+ concentrations (200 mM, pH 4.0). At steady state, KcsA gating is dominated by very long silent periods ($\tau > 25$ s) interrupted by bursts of openings of highly variable kinetics (mean open times vary between 5 and 100 ms). P_o varies between 0.05 and 0.15 ($n > 40$ patches).

[1]Department of Molecular Physiology and Biological Physics, University of Virginia, Charlottesville, Virginia 22906, USA. [2]Department of Physiology & Biophysics, Weill Medical College of Cornell University, 1300 York Avenue, New York, New York 10021, USA. [3]Present address: Institute of Molecular Pediatrics Science and Department of Biochemistry and Molecular Biology, University of Chicago, Center for Integrative Science, 929 East 57th Street, Chicago, Illinois 60637, USA. Correspondence should be addressed to E.P. (eperozo@virginia.edu).

Received 18 October 2005; accepted 18 January 2006; published online 12 March 2006; doi:10.1038/nsmb1069

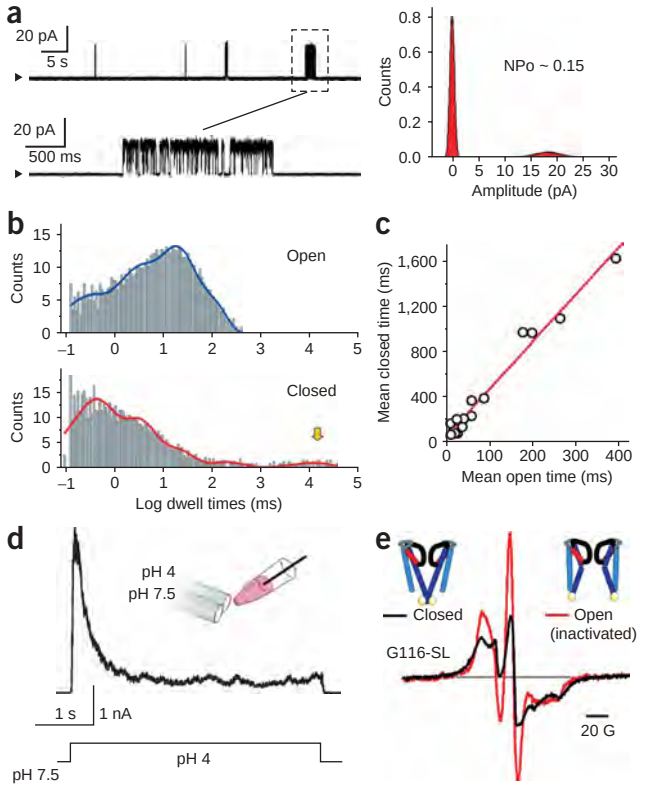

Figure 1 KcsA is inactivated under steady-state conditions. (**a**) Single-channel recordings of KcsA obtained in symmetric KCl solutions (200 mM, pH 4) are dominated by long closures. Left, traces shown in a slow time scale (top) and as a higher-resolution detail (bottom). Right, all-points histogram. Gaussian fits to the individual peaks were used to determine the nominal open probability (NPo = 0.15). (**b**) Dwell-time distributions at +150 mV and pH 4.0 for a representative single-channel recording of KcsA. Yellow arrow points to the dominant closed time. (**c**) A linear correlation exists between mean open and closed times for KcsA gating as well as for the wide-range variation in the individual patches (each symbol represents a different experiment). (**d**) KcsA macroscopic currents activated by a rapid pH jump reveal the presence of a time-dependent inactivation process. Inset diagram represents the rapid solution exchange. (**e**) Opening of the intracellular gate of KcsA monitored by CW-EPR from spin labels attached at residue G116C (G116-SL). Shown are CW-EPR spectra obtained after equilibrating reconstituted channels in pH 7 (black trace) or pH 4 (red trace) solution.

KcsA dwell-time distributions reveal a complex, multiexponential behavior (**Fig. 1b**), which for the open times is mostly populated by transitions in the 5- to 20-ms range and for the closed times by intraburst closures with time constants of 0.5–10 ms.

Kinetic variability seems to be a hallmark of KcsA gating. This variability seems to occur in a nonrandom fashion, as evidenced by the existence of a linear relationship between mean open and mean closed times across a large set of individual patches (**Fig. 1c**). This relationship suggests that for patches with a wide range of kinetics, long open times are typically associated with very long closed periods, as expected if the molecular determinants of steady-state gating occur within a unique and well-defined region of the protein. We reasoned that this phenomenon could be explained by association of the long silent times in KcsA not with a resistance to opening at low pH, but with the presence of a previously unrecognized inactivated state. The possibility of C-type inactivation in KcsA was first suggested by experiments with Shaker-KcsA chimeras[30], but these results were indistinguishable from pore-blockage effects.

The inactivation process is best revealed under nonstationary conditions. Therefore, we performed pH-jump experiments using KcsA reconstituted at high protein-to-lipid ratios to study the time course of macroscopic currents. At depolarized voltages and in symmetric K^+ solutions (200 mM), changing the bath pH from 7.5 to 4.0 produced large, highly reproducible K^+ current transients (**Fig. 1d**). These transients were characterized by a relatively fast activation time course ($t \sim$ 10–20 ms), followed by an exponential decay with a single time constant between 0.5 and 1.5 s relaxing to a steady-state current that represented only 5%–10% of the peak current

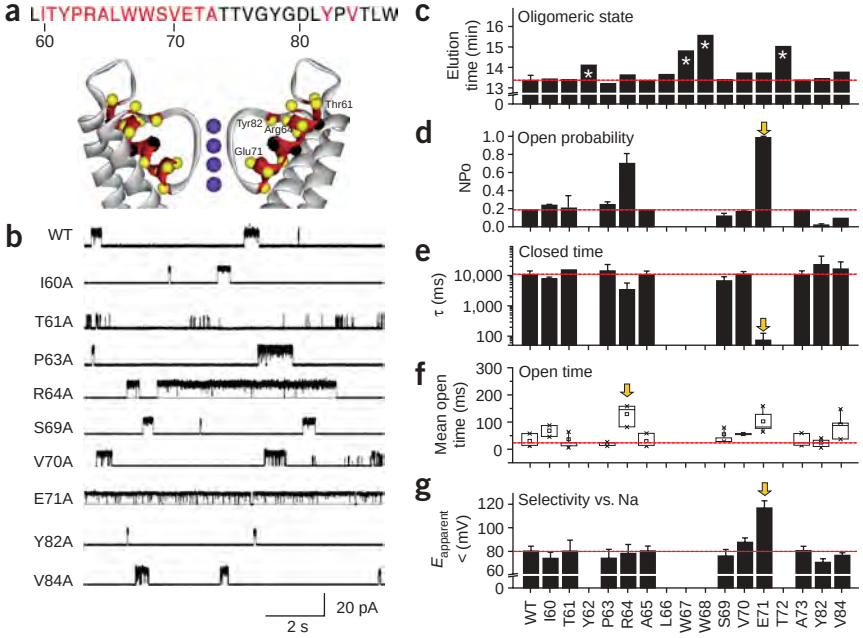

Figure 2 A pore-loop alanine scan identifies residues crucial for the inactivation event. (**a**) Top, P-loop sequence with alanine mutations in red. Bottom, locations of the mutated residues in the KcsA structure (yellow spheres). Residues in black represent positions for which data were not obtained. (**b**) Representative single-channel traces of the alanine mutants obtained at pH 4 and +150 mV in symmetric K^+ solutions. (**c**) Hydrodynamic properties of the alanine mutants evaluated from the peak elution time of the KcsA tetramer in a Superdex 200 gel-filtration column. (**d**) Nominal open-channel probability evaluated from Gaussian fits of all-points histograms. (**e**) Dominant (slowest) closed-time constant as determined from nominally single-channel traces. (**f**) Box plot of mean open times. In panels **c**–**g**, dotted red line represents the mean value of WT KcsA. (**g**) Selectivity versus Na^+ estimated from single-channel I-V ramps under bi-ionic conditions. No detectable Na^+ currents were seen in any of the mutants. $E_{apparent}$ is the potential at which K^+ currents can last be resolved. Error bars show s.d.

value. Recent preliminary analyses of KcsA expressed in mammalian cells have shown a very similar behavior[31]. Consequently, the EPR spectroscopic change detected at low pH (**Fig. 1e**) is dominated by conformations in which the intracellular gate is structurally open, but the channel is functionally inactivated.

The inactivation gate is located at the selectivity filter

We next aimed to identify the regions of KcsA responsible for the inactivation process. We focused our attention on the P-loop (**Fig. 2a**) by performing an alanine scan at the pore helix (residues 60–73) and the extracellular vestibule of the pore (residues 82 and 84), analyzing the steady-state single-channel properties of each stable mutant at low pH (**Fig. 2b**). We avoided residues involved in ion conduction (74–81) and rejected mutants whose oligomeric hydrodynamic properties deviated from the behavior of wild-type channels (**Fig. 2c**).

An overview of the single-channel traces reveals that the majority of the investigated alanine mutants show gating behaviors similar to that of the wild-type channel. As in wild-type (WT) KcsA, most of the mutants have low open probabilities, very long closures and mean open times that vary between 5 and 30 ms (**Fig. 2d–f**). However, we identified three P-loop mutants that fundamentally affected KcsA gating: R64A, E71A and Y82A. In all cases, channels were fully selective against Na^+ under bi-ionic conditions (no Na^+ currents were detected), although we found slight shifts in the apparent reversal potential (**Fig. 2g**) for E71A (more selective) and Y82A (less selective) relative to the wild-type channel.

By far the most dramatic functional effect was observed upon placing an alanine at position Glu71. This mutant consistently showed extremely high open probabilities ($P_o \sim 0.95$–0.99). Moreover, this was the only mutation that completely abolished the characteristic long closures associated with the low P_o in KcsA (**Fig. 2e**), rendering this mutant constitutively open at low pH. The E71A mutation also flattens the mean open versus mean closed time relationship (**Fig. 3a**, red circles) relative to that in WT KcsA (black squares) and, as expected, produces non-inactivating macroscopic currents in pH-jump experiments (**Fig. 3b**, red trace). The high-resolution KcsA structure[32] has shown that E71 forms a strong carboxyl-carboxylate interaction with position Asp80 at the end of the Gly-Tyr-Gly-Asp signature sequence. This interaction is present in other bacterial channels[33], and related electrostatic interactions exist in inward rectifiers[34], but it is not normally found in eukaryotic voltage-gated channels. Although this interaction has important consequences for thermal stability in KcsA[35], its precise functional role has been less obvious. Functional studies of mutation E71V using planar lipid bilayers have found some permeability differences from WT KcsA, but no major effects on steady-state gating[35]. However, although we can reproduce the changes in E71V permeation, we find that under the present experimental conditions this mutation also has a dramatic influence on gating, increasing overall P_o via a decrease in the rate of inactivation (data not shown). The origin of this discrepancy is yet to be determined.

Substituting an alanine at position Arg64 increases the steady-state P_o to about 0.65. This increase in single-channel activity is the consequence of a relatively small decrease in the dominant closed dwell time (**Fig. 2e**) and an overall increase in the mean open time (**Fig. 2f**). After pH jumps, macroscopic currents show that the inactivation process is still present in R64A, but it proceeds at an intermediate rate between those of WT KcsA and E71A (**Fig. 3b**, blue trace). In contrast, substitution of Tyr82 for alanine decreases open probability ($P_o \sim 0.01$) relative to that of WT KcsA by lengthening the long closures and thus further stabilizing the inactivated state (**Fig. 2e**). This is shown in

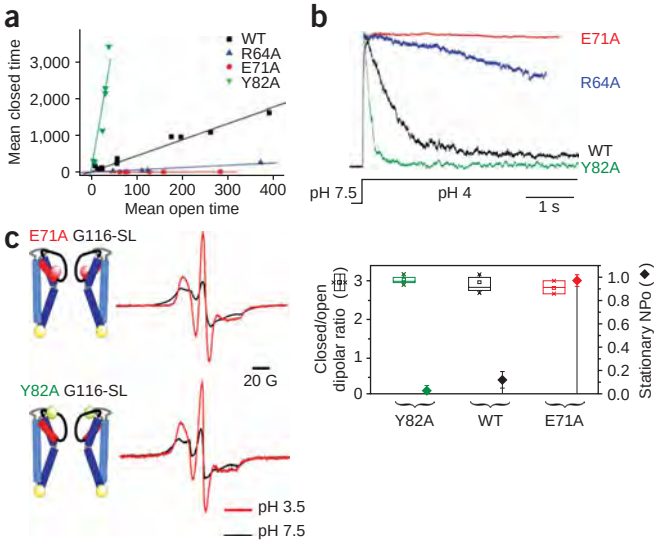

Figure 3 Pore-loop mutants influence the rate and extent of inactivation. (**a**) The mean open versus mean closed times plot for E71A loses the linear correlation seen for WT KcsA, but Y82A promotes inactivation and suggests a common mechanism with C-type inactivation. (**b**) Normalized macroscopic currents from rapid pH jumps show the almost complete elimination of the time-dependent inactivation process in E71A, a sharp reduction of inactivation for R64A and an enhancement of the rate and extent of inactivation for Y82A. (**c**) The magnitude of the conformational rearrangement at the intracellular gate does not govern the steady-state open probability. Gating changes were monitored by CW-EPR from spin labels attached at residue G116C (G116-SL) in wild-type channels and in mutants with very low (Y82A) and very high (E71A) P_o. Left, CW EPR spectra of the spin-labeled double mutants E71A G116C and Y82A G116C at neutral (black trace) and acidic (red trace) pH conditions. Right, the extent of intracellular gate opening derived from the amplitude ratio of spectra (dipolar ratio Ω; box plot) is identical in WT, Y82A and E71A, in spite of large differences in P_o associated with the gating of each mutant (diamonds). Error bars show s.d.

Figure 3b, where macroscopic inactivation is both considerably faster and more complete after a rapid pH jump (green trace).

The present alanine scan has helped identify three KcsA mutants that have a wide variety of steady-state open probabilities. We took advantage of this set of mutants to evaluate the relative contributions of the selectivity filter and the inner helix bundle gate to steady-state gating. To this end, we introduced the E71A or Y82A mutations into a KcsA background with mutation G116C. This cysteine serves as a spin-labeling site to report on the pH-dependent conformational changes in TM2 (refs. 8,9). Comparison of the continuous-wave EPR (CW-EPR) spectra for spin-labeled G116C, E71A G116C and Y82A G116C mutants at pH 7.5 and 3.5 revealed strikingly similar spectral changes (**Fig. 3c**, left). Furthermore, the magnitude of the opening at the helical-bundle crossing (estimated from the dipolar spectral amplitude ratio; **Fig. 3c**, right, box plot) does not change, in spite of the fact that these channels gate with a difference in steady-state nominal open probability (NPo) of two orders of magnitude (**Fig. 3c**, right, diamonds). This result supports the argument that, once activated by protons, the TM2 gate fully opens at low pH, in spite of widely differing patterns of single-channel behavior, and it shows that most of the steady-state gating activity in KcsA takes place at the selectivity filter.

Several lines of evidence point to a mechanistic equivalence between this KcsA inactivation mechanism and the C-type inactivation process associated with voltage-dependent channels. One of the hallmarks of C-type inactivation is its dependence on external K^+ concentration[29].

Here, pH-jump experiments carried out in the presence of extracellular *N*-methylglucamine (NMG) (200 mM) show that the rate of inactivation is faster than in symmetric K^+ (see **Supplementary Figure 1** online). This result points to the well-known role of the external K^+-binding site in stabilizing the conductive conformation of the pore. Residue Tyr82 in KcsA is functionally equivalent to Thr449 in Shaker; mutation of the latter to alanine dramatically accelerates C-type inactivation[29], as observed in KcsA (**Fig. 3b**). Furthermore, mutations of Ser620 in hERG (equivalent to position 71 in KcsA) have a large impact on the rate of C-type inactivation[36]. These observations also agree with the known changes in K^+/Na^+ selectivity found in C-type–inactivating channels[27] and the alanine mutants that relieve or promote inactivation (**Fig. 2g**).

Two crystal structures of the E71A mutant

We determined the atomic structure of the E71A KcsA mutant to establish whether the large increase in open probability is reflected in the conformation of the filter. The structure of the E71A mutant in complex with a Fab antibody was solved by molecular replacement using the WT KcsA–Fab structure (PDB entry 1K4C)[32] as the search model. Of multiple diffracting crystals examined (resolution up to 2.5 Å), two X-ray structures of E71A–Fab were determined (**Fig. 4**). One structure is quite similar to WT KcsA, whereas the other shows substantial conformational changes in three regions of the pore: the selectivity-filter backbone, Asp80 at the outer end of the pore and Trp67 along the pore helix.

We refer to these two X-ray structures as the 'flipped' and 'nonflipped' conformations, according to the extent to which the side chain of residue Asp80 moves upward relative to its position in the WT structure (see below). The final models for these two structures were refined to free and crystallographic *R*-factors of 24.2% and 26.3%, respectively, for flipped E71A, and 24.3% and 25.6%, respectively, for nonflipped E71A. The model of the flipped Fab–E71A complex contains 534 amino acid residues, 43 water molecules, one partial lipid and six K^+ ions. The nonflipped model contains 534 amino acids, 32 water molecules, two partial lipids and seven K^+ ions. **Figure 4a** shows the electron density ($2F_o - F_c$ map) and fitted model for the flipped E71A structure in the region around the selectivity filter. The shorter alanine side chain at position 71 leaves a space of nearly 90 $Å^3$ where no crystallographic water molecules were detected. This cavity could presumably be filled by 3 ± 1 water molecules on average (see Methods).

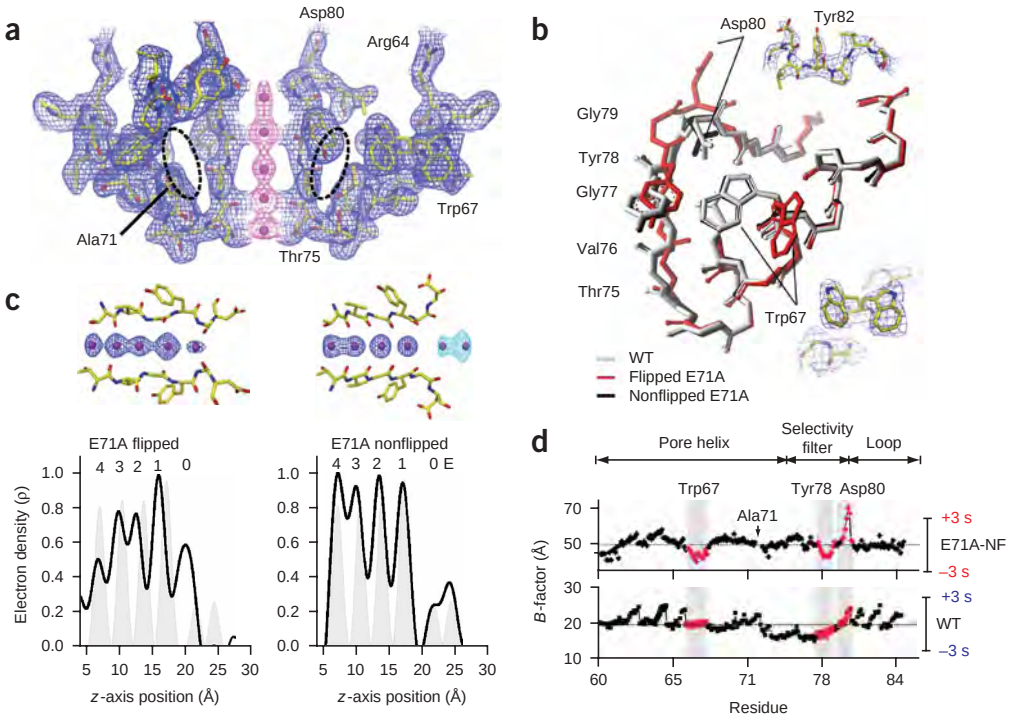

Figure 4 Two crystal structures of the E71A mutant. (**a**) Electron density map of residues 60–84 from two diagonally symmetric subunits for the crystal form of E71A with residue Asp80 flipped upward (flipped E71A). Sticks, polypeptide chain; blue mesh, 1-σ contour of the $2F_o - F_c$ electron density map for the protein; magenta mesh, 2-σ contour of the ions; black dotted ovals, cavities created by the absence of the Glu71 side chain. (**b**) Single-subunit line representation of the P-loop of the flipped (red) and nonflipped (black) E71A structures overlaid onto the wild-type structure[32] (PDB entry 1K4C; gray) highlights the conformational rearrangements in the backbone of the selectivity filter (residues 75–79). Insets, the side chain conformational changes in Asp80 and Trp67 as fitted to the 2-σ contour of the simulated annealing omit map. The omit maps were calculated for residues 79–84 and 67, respectively; atoms within 3.5 Å of selected residues were also omitted in the calculation. The density attributed to the alternate rotamer of the Trp67 side chain in the flipped X-ray structure is clearly distinct from the density of the lipid observed near this position in the WT X-ray structure[33]. (**c**) One-dimensional electron density profiles for the two crystal conformations of the E71A mutant (flipped and nonflipped). Top, $F_o - F_c$ omit maps of K^+ ions in the selectivity filter shown relative to the protein model. The electron density maps are shown as a 6-σ contour for the flipped E71A conformer and as 7-σ (blue) and 4-σ (cyan) contours for the nonflipped E71A conformer. Different contour levels were chosen for the purpose of visual clarity. Bottom, one-dimensional electron density profile along the central symmetry (*z*) axis is shown using the ion in the cavity as $z = 0$. Gray-shaded peaks represent the profile for the wild-type channel (PDB entry 1K4C at 2.0 Å). Numbers and E at top denote the K^+-binding sites (S0–S4 and S_{ext}, respectively).(**d**) Comparison of crystallographic *B*-factors for P-loop residues (63–83) from the WT KcsA structure (bottom chart) and the nonflipped E71A mutant (E71A-NF, top chart). Black dotted line represents the mean value for all atoms in the P-loop. Vertical capped lines represent the ±3 σ values for each data set.

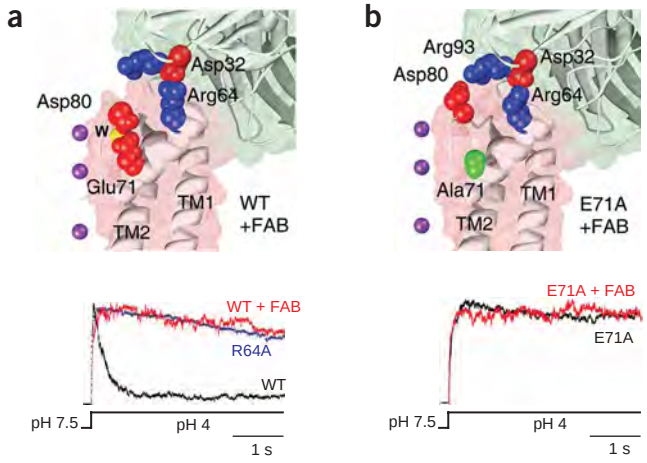

Figure 5 Influence of Fab fragment binding on KcsA gating. (**a**) Effect of Fab binding on wild-type KcsA. Top, macroscopic K^+ currents after a rapid pH jump (from 7.5 to 4) were obtained from proteoliposomes containing reconstituted KcsA or the KcsA–Fab complex (traces normalized to peak amplitude). Bottom, ion pairing between Arg64 in KcsA and Asp32 (CPK representation) in Fab as a possible basis for stabilization of the selectivity filter in the conductive conformation. (**b**) Fab effects on the E71A mutant. Top, macroscopic K^+ currents after a rapid pH jump, as in **a**. Bottom, the increased flexibility of Asp80 in the absence of Glu71 places its carboxyl moiety within ion-pair range of residue Arg93 in Fab, leading to a conformational trap of the Asp80-flipped conformation. Figure was prepared with UCSF Chimera[50].

Superposition of the E71A and WT KcsA structures reveals the details of the conformational rearrangements found in the mutant (**Fig. 4b**). The r.m.s. deviation of the flipped E71A relative to the WT structure is 1.21 Å for the backbone of residues 62–82 (1.61 Å when the side chains are included). The nonflipped conformation is quite similar to WT, with only small structural changes around the selectivity filter (backbone r.m.s. deviation of 0.25 Å relative to WT for residues 62–82). Nonetheless, a slight upward displacement of the carboxylate side chain of residue Asp80 of ~0.5 Å toward the extracellular side is observed. In contrast, the carboxyl side chain of Asp80 moves upward by ~8 Å in the flipped conformation (**Fig. 4b**, upper inset). Perhaps as a consequence of this large reorientation, the backbone of residues 75–81 shows major reorientations, particularly for residues 79–80, where the backbone is displaced upward over 2 Å, and residues Val76 and Tyr78, where backbone carbonyls reorient away from the four-fold axis of symmetry. Changes in the backbone of the pore helix appear minimal, though electron density corresponding to two distinct rotamers for Trp67 is clearly observed.

The structural rearrangements observed in the flipped E71A structure have an impact on the position and occupancy of the ions in the selectivity filter. **Figure 4c** shows the electron density for the ions in the pore for the flipped (left) and nonflipped conformations. In the flipped conformation, the ions in the S1 to S3 binding sites appear displaced by about 1.5 Å toward the intracellular side of the pore, with one additional ion density present between residues 78 and 79. It is unclear whether this position corresponds to a transitioning ion between S1 and S0. In the flipped conformation, there is little or no density corresponding to the external ion-binding sites (S0 and S_{ext})[32]. One-dimensional electron density profiles along the pore axis (**Fig. 4c**, bottom) for the two crystal conformations of the E71A mutant confirm that ions in the nonflipped structure match the positions and occupancy of those in the wild-type structure. However, the ion occupancy in the flipped structure shows a higher occupancy of S1 relative to S2–S4. This result was somewhat unexpected, given that the largest distortions in the selectivity-filter backbone occur precisely near the S1 binding site.

Comparing the crystallographic *B*-factors in the E71A structures with those of the wild-type channel provides useful clues to the possible mechanism behind open-channel stabilization. Comparing absolute *B*-factors for structures of different resolutions is particularly complicated because of the uncertainty in determining the relative contributions from local dynamics and lattice disorder[37]. We have minimized this issue by comparing the relative variations of the *B*-factors around the local means for specific regions of the protein. **Figure 4d** shows a comparison of the crystallographic *B*-factors of the wild-type structure and the nonflipped E71A structure (residues 63–83) relative to their respective local mean values (dotted lines). In the mutant, there is a considerable increase in the *B*-factors for residues Asp80 and Arg64 (>4 σ values), whereas Trp67 shows a significant decrease in its *B*-factor values (about 3 σ). Notably, the *B*-factor plot of the nonflipped E71A structure shows approximately the same behavior as that of the flipped structure (data not shown), a

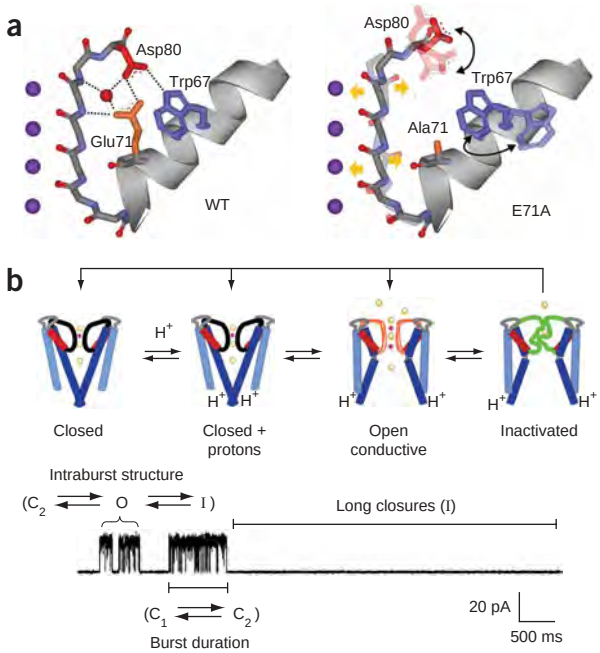

Figure 6 A mechanistic interpretation of KcsA gating. (**a**) Possible mechanism of action of the E71A mutation in stabilizing the open state. A single-subunit P-loop is shown with positions 67, 71 and 80 in stick representation. In the wild-type channel (left), the interaction between Asp80 and Trp67 destabilizes the conductive conformation of the filter and promotes inactivation through an as yet unknown mechanism. Eliminating the Asp80-Glu71 carboxyl-carboxylate (E71A, right) disrupts the hydrogen bonding network between the signature sequence (Gly-Tyr-Gly-Asp) and the pore helix, causing an increase in Asp80 dynamics and perturbing the Asp80-Trp67 interaction. This sharply decreases entry into the inactivated state, stabilizing the open state. (**b**) Top, cartoon representation of the structural conformation associated with each kinetic state. Bottom, correlation of specific kinetic transitions with KcsA single-channel behavior. Because stationary gating is dominated by the deeply inactivated state, single-channel openings occur mainly as a result of rare returns from the inactivated state owing to conformational changes in the selectivity filter while the lower gate remains open.

fact that supports the idea that that the two structures, although different, may represent distinct conformational snapshots of a common functional state.

Functional consequences of Fab binding

The *B*-factor analysis suggests that the conformational fluctuations in the neighborhood of the selectivity filter are correlated through a delicate network of inter- and intrasubunit interactions. This raises issues about the influence of Fab antibody on the conformations observed in the crystal structures of KcsA. Examination of the interacting surface between the channel and the antibody reveals the presence of a well-defined salt bridge between residues Asp32 in the B chain of Fab and Arg64 at the N-terminal end of the pore helix (**Fig. 5a**, top). It might be recalled that besides Glu71, Arg64 is the only position along the pore helix that generates major increases in the steady-state P_o, having an influence on both open and closed times (**Fig. 2e**,**f**). We addressed this issue by recording macroscopic KcsA currents of the reconstituted WT KcsA–Fab complex after fast pH jumps. The presence of the antibody substantially reduces inactivation and stabilizes the channel in its conductive state (**Fig. 5a**, bottom, red trace). Because the structures of WT KcsA with[32] and without[38] antibody are essentially the same, this result suggests that although the TM2 gate remains closed in the X-ray structure, the Fab-stabilized conformation of the selectivity filter might be a conductive or preconductive state. This conclusion is consistent with the results of molecular dynamics computations showing that there are no large free-energy barriers opposing K^+ movements when the filter is in the conformation of the X-ray structure of the wild-type channel[39].

Macroscopic currents of the reconstituted E71A–Fab complex (**Fig. 5b**) showed little additional effect on the non-inactivating current, suggesting that the antibody does not exert secondary gating effects. Notably, examination of the flipped E71A–Fab interface reveals that the reorientation and stabilization of Asp80 is probably the result of an electrostatic interaction with position Arg93 in Fab (**Fig 5b**, top). We interpret this finding to suggest that, during gating, residue Asp80 populates a wide range of conformations both in the wild-type channel and in the E71A mutant. The presence of the antibody helps stabilize one particular conformation of the filter. Thus, although Asp80 could move up to ~8 Å, the antibody itself is probably trapping the filter in the 'extreme' conformation where Asp80 interacts with Arg93 in Fab.

DISCUSSION

A mechanistic interpretation of KcsA gating

The finding of a time-dependent inactivation process forces a reinterpretation of KcsA gating as we understand it. It has long been assumed that the low P_o and long closed times were a consequence of inefficiency in the coupling between proton binding and gate opening, reflecting the limited rates of the transitions between closed and open states. The present results reveal that, in fact, proton activation is likely to be very efficient and that the dominant opening gating transition in KcsA under steady-state conditions is not the closed-open equilibrium but the partial recovery from a previously unrecognized C-type–inactivated state. This finding also seems to settle the KcsA gating paradox, as it is clear that opening of the intracellular gate is not the only determinant of steady-state open probability in KcsA.

On the basis of the present set of results, we propose that the conductive conformation of the filter, represented by the wild-type structure[32], is intrinsically unstable owing to the destabilizing interactions between Asp80 and Trp67, Asp80 and Glu71, or both (**Fig. 6a**, left). Therefore, eliminating the carboxyl-carboxylate interaction between Asp80 and Glu71 (**Fig. 6a**, right) increases the flexibility of the side chain of Asp80, weakening its (disruptive) hydrogen bonding interactions with Trp67, which is thereby able to undergo a reorientation between two rotamers with similar energies. The relative decrease in the *B*-factors of Trp67 in the X-ray structure of the E71A mutant (**Fig. 4d**) is consistent with this hypothesis.

The current data can be framed into an explicit mechanistic model of KcsA gating that correlates specific structural snapshots with a sequence of kinetically defined events (**Fig. 6b**). This model allows for a direct correlation with the key features of KcsA macroscopic and single-channel activity. Hence, the stimulus-dependent gate (TM2) is predicted to be a determinant in the duration of individual open-channel bursts from transitions among closed states and the open state ($C_1 \leftrightarrow C_2 \leftrightarrow O$). However, the rapid intraburst behavior is mostly defined by the $O \leftrightarrow I_1$ equilibrium, whereas the long closures arise from transitions to the long-lived inactivated state I_2. Removal of the Glu71-Asp80 interaction in the E71A mutant prevents the transition to I_2, unmasking the gating events of the $O \leftrightarrow I_1$ equilibrium at steady state.

The functional state of the flipped E71A structure is not clear at this time. Electrophysiological data demonstrate that the E71A mutant spends most of its time in the conductive conformation. This is compatible with the structural similarity between WT KcsA and the non-flipped E71A, given that molecular dynamics calculations have shown that these conformations do not contain large energy barriers to ion translocation[39]. However, the large backbone rearrangements observed in the flipped E71A structure together with the observed changes in ion position and occupancy suggest that the conductive state of the selectivity filter may be supported by a wide range of conformations. It is tempting to suggest that the flipped E71A structure represents an intermediate conductive conformation. Whether the intermediate is within the range of possible open states or even a transition to the inactivated state is unclear and will require further investigation.

The stabilization of the conductive state of the channel by Fab has important implications concerning the interpretation of the available high-resolution structures of the selectivity filter in terms of putative inactivated states. It has been shown that the KcsA filter changes its conformation (and the number of coordinated ions) when the K^+ concentration is below 20 mM[32,40]. However, it is unlikely that this structural change corresponds to the inactivated state, as KcsA readily inactivates even when the selectivity filter is saturated with K^+ ions. Similarly, the conformational rearrangements observed in a recent KcsA structure obtained in the presence of bound tetra-butylammonium is unlikely to represent a C-type–inactivated state as claimed[41]. The influence of the KcsA-Fab interaction on the inactivation process (**Fig. 5a**) leads us to think that this structure might correspond to only a partial conformational change toward the C-type–inactivated state. Determination of the structure of the inactivated filter will probably require a high-resolution KcsA structure with a different or modified Fab antibody.

Although more work will be required to fully characterize all the functional states of the channel, the present results make it clear that the selectivity filter can undergo much larger conformational excursions than previously suggested. The present X-ray structures gives us a hint of the range of possible selectivity-filter conformations associated with transitions between closed, open and inactivated states.

METHODS

Mutagenesis and channel biochemistry. Channels were mutated, expressed and purified as previously described[8,43] using a pQE32 vector containing KcsA with the RGS-His_6 epitope at the N terminus. KcsA was solubilized in PBS

containing dodecyl maltoside at room temperature, spun down at 100,000*g* for 1 h and purified with a Co^{2+}-based metal-chelate chromatography resin (Talon resin, Clontech). For EPR measurements, the purified mutant proteins were spin-labeled with methanethiosulfonate spin label (Toronto Research) at a 10:1 label/channel molar ratio and reconstituted in either asolectin vesicles (for patch-clamp experiments) or a POPC18/POPG18 ratio of 3:1 by dilution in PBS followed by additional detergent extraction with biobeads[4].

Liposome patch clamp. Electrophysiological measurements on liposome-reconstituted KcsA were done by patch-clamp techniques following the method of ref. 42 with previously described modifications[44]. Single-channel traces were obtained from channels reconstituted at a 1:10,000 protein/lipid ratio (mass/mass). Under these conditions, less than 50% of the patches showed any single-channel activity. Macroscopic currents were measured at a 1:100 ratio. The liposome suspension was centrifuged for 1 h at 100,000*g* and the pellet (about ~10 mg of lipids) was resuspended in 60 µl of rehydration buffer. The proteoliposomes were dried overnight in a desiccation chamber under vacuum and then rehydrated with 20 µl of buffer, yielding liposomes suitable for patch-clamp experiments after a few hours. Unless explicitly stated, patch-clamp measurements were done in symmetrical conditions: 200 mM KCl and 4-morpholine propanesolfonic acid (MOPS) buffer at pH 4.0 at room temperature. Bi-ionic experiments for selectivity measurements were obtained using 1.2-s ramps between –200 and +200 mV. Single-channel currents were recorded with a Dagan 3900 patch-clamp amplifier, and currents were sampled at 40 kHz with an analog filter set to 5 kHz (–3 dB). Pipette resistances were 1–2 MΩ. Macroscopic currents were recorded after a pH jump using an RCS-160 fast solution exchanger (Biologic) fed by gravity.

Single-channel analysis and kinetic modeling. Single-channel data were filtered at 5 kHz (8-pole Bessel) and digitized at a sampling rate of 40 kHz. Single-channel kinetic analyses were done using pCLAMP 9 (Axon Instruments). Idealization of the currents was done through the half-amplitude threshold algorithm at 2 kHz. Owing to the difficulties associated with estimating the number of active channels in patches of low P_o (all but those from R64A and E71A), individual values for the dominant closed time constant (**Fig. 2e**) must be considered as a lower-limit estimate, and some of the variability among the different mutants (except E71A) could derive from underestimating channel number.

EPR spectroscopy. X-band CW-EPR spectra were obtained from spin-labeled and reconstituted channels as described in ref. 8 in a Bruker ELEXYS spectrometer equipped with a loop-gap resonator under the following conditions: 2 mW incident power, 100-kHz modulation frequency and 1-G modulation amplitude. All spectra were obtained at room temperature.

X-ray crystallography. The KcsA mutant protein E71A was crystallized in the presence of an antibody Fab fragment following published protocols[32,38]. Beam-like crystals of KcsA–Fab complex appeared after 1 week in a sitting drop containing 20%–25% (v/v) PEG 400, 50 mM magnesium acetate and 50 mM sodium acetate (pH 5.4–5.6) at 20 °C. Crystals diffracted to Bragg spacing of 2.5 Å for the KcsA–Fab complex crystals. Data collection and refinement statistics are given in **Table 1**. Data were obtained at the X4a and X29 beamlines of the National Synchrotron Light Source and processed with DENZO and SCALEPACK[45]. E71A structures were solved by molecular replacement using the WT KcsA–Fab complex structure (PDB entry 1K4C) as a search model. Refinement of the structures was carried out through multiple cycles of manual rebuilding using O[46] and refinement using CNS[47]. *B*-factor refinement was carried out using the script of individual *B*-factor refinement (bindividual.inp) in CNS with default settings and maximum-likelihood refinement target using amplitudes. In the first round of refinement, the *B*-factors for all atoms were reset to the value of 50.0 (ref. 32). One-dimensional electron density profiles along the central axis of the selectivity filter were obtained as described in ref. 40.

Molecular dynamics and grand canonical Monte Carlo calculations. The simulations were carried out using CHARMM as described previously[48]. To efficiently sample the configuration and occupancy of water molecules confined within the empty space left by the substitution of Glu71 by an alanine, we used a grand canonical Monte Carlo algorithm[49]. Upon analyzing 50 ps of simulation (10,000 grand canonical Monte Carlo steps for every 5 ps dynamics), we found that the void can be accommodated by an average of three or four water molecules (including the crystallographic water). To further establish the structural importance of water molecules in this cavity, we carried out molecular dynamics simulations of 2 ns on the E71A mutant with one, two and three water molecules. The filter is most stable in the system during the trajectory with three water molecules. The trajectories with one or two water molecules resulted in flipping of the Val77 carbonyl in one of the four subunits.

Table 1 Data collection and refinement statistics

	E71A nonflipped	E71A flipped
Data collection		
Space group	*I*4	*I*4
Cell dimensions		
a, *c* (Å)	155.98, 75.96	155.16, 75.72
Resolution (Å)	50.0–2.5	50.0–2.5
R_{sym} or R_{merge} (%)	6.75 (45.3)	6.90 (57.1)
I / σI	41.4 (1.9)	27.2 (2.4)
Completeness (%)	89.2 (48.6)	96.4 (91.9)
Redundancy	6.5	3.9
Refinement		
No. reflections	27,186	25,067
R_{work} / R_{free} (%)	24.3 / 25.6	24.2 / 26.3
No. atoms		
Protein	4,065	4,070
Ligand/ion	17	17
Water	37	43
B-factors		
Protein	83.39	64.23
Ligand/ion	102.53	85.79
Water	72.55	62.60
Bond lengths (Å)	0.008	0.007
Bond angles (°)	1.390	1.381

Each data set was collected from a single crystal frozen in liquid nitrogen. Highest-resolution shell is shown in parentheses.

Accession codes. Protein Data Bank: Coordinates have been deposited with accession codes 1ZWI for the nonflipped E71A structure and 2ATK for the flipped structure.

Note: Supplementary information is available on the Nature Structural & Molecular Biology website.

ACKNOWLEDGMENTS

We thank J. Bushweller, R. Nakamoto and S. Chakrapani for critically reading the manuscript; the staff at BNL X-4A and X-29 for assistance in data collection; R. MacKinnon (Rockefeller University) for providing the KcsA monoclonal antibody hybridoma cell line and F.W. Garcia for assistance with monoclonal antibodies; and H. Wu for generous access to her laboratory space and facilities. V. Vasquez provided assistance with mutagenesis and channel biochemistry; C. Gonzalez provided comments and experimental advice. This work was supported by grants from the US National Institutes of Health to E.P. and B.R.

COMPETING INTERESTS STATEMENT

The authors declare that they have no competing financial interests.

Published online at http://www.nature.com/nsmb/
Reprints and permissions information is available online at http://npg.nature.com/reprintsandpermissions/

1. MacKinnon, R. Potassium channels and the atomic basis of selective ion conduction. *Angew. Chem. Int. Edn Engl.* **43**, 4265–4277 (2004).
2. Yellen, G. The voltage-gated potassium channels and their relatives. *Nature* **419**, 35–42 (2002).

3. Schrempf, H. *et al.* A prokaryotic potassium ion channel with two predicted transmembrane segments from *Streptomyces lividans*. *EMBO J.* **14**, 5170–5178 (1995).
4. Cuello, L.G., Romero, J.G., Cortes, D.M. & Perozo, E. pH-dependent gating in the *Streptomyces lividans* K^+ channel. *Biochemistry* **37**, 3229–3236 (1998).
5. Heginbotham, L., LeMasurier, M., Kolmakova-Partensky, L. & Miller, C. Single *Streptomyces lividans* K^+ channels: functional asymmetries and sidedness of proton activation. *J. Gen. Physiol.* **114**, 551–560 (1999).
6. Cordero, J.F., Cuello, L.G. & Perozo, E. Voltage-dependent gating at the KcsA selectivity filter. *Nat. Struct. Mol. Biol.*, advance online publication 12 March 2006 (doi:10.1038/nsmb1070).
7. Liu, Y.S., Sompornpisut, P. & Perozo, E. Structure of the KcsA channel intracellular gate in the open state. *Nat. Struct. Biol.* **8**, 883–887 (2001).
8. Perozo, E., Cortes, D.M. & Cuello, L.G. Three-dimensional architecture and gating mechanism of a K^+ channel studied by EPR spectroscopy. *Nat. Struct. Biol.* **5**, 459–469 (1998).
9. Perozo, E., Cortes, D.M. & Cuello, L.G. Structural rearrangements underlying K^+-channel activation gating. *Science* **285**, 73–78 (1999).
10. Hackos, D.H., Chang, T.H. & Swartz, K.J. Scanning the intracellular S6 activation gate in the shaker K^+ channel. *J. Gen. Physiol.* **119**, 521–532 (2002).
11. Jin, T. *et al.* The $\beta\gamma$ subunits of G proteins gate a K^+ channel by pivoted bending of a transmembrane segment. *Mol. Cell* **10**, 469–481 (2002).
12. Liu, Y., Holmgren, M., Jurman, M.E. & Yellen, G. Gated access to the pore of a voltage-dependent K^+ channel. *Neuron* **19**, 175–184 (1997).
13. Loussouarn, G., Phillips, L.R., Masia, R., Rose, T. & Nichols, C.G. Flexibility of the Kir6.2 inward rectifier K^+ channel pore. *Proc. Natl. Acad. Sci. USA* **98**, 4227–4232 (2001).
14. Jiang, Y. *et al.* The open pore conformation of potassium channels. *Nature* **417**, 523–526 (2002).
15. Jiang, Y. *et al.* X-ray structure of a voltage-dependent K^+ channel. *Nature* **423**, 33–41 (2003).
16. Meuser, D., Splitt, H., Wagner, R. & Schrempf, H. Exploring the open pore of the potassium channel from *Streptomyces lividans*. *FEBS Lett.* **462**, 447–452 (1999).
17. Demo, S.D. & Yellen, G. Ion effects on gating of the Ca^{2+}-activated K^+ channel correlate with occupancy of the pore. *Biophys. J.* **61**, 639–648 (1992).
18. Shapiro, M.S. & Decoursey, T.E. Selectivity and gating of the type-L potassium channel in mouse lymphocytes. *J. Gen. Physiol.* **97**, 1227–1250 (1991).
19. Spruce, A.E., Standen, N.B. & Stanfield, P.R. Rubidium ions and the gating of delayed rectifier potassium channels of frog skeletal-muscle. *J. Physiol. (Lond.)* **411**, 597–610 (1989).
20. Swenson, R.P., Jr & Armstrong, C.M. K^+ channels close more slowly in the presence of external K+ and Rb+. *Nature* **291**, 427–429 (1981).
21. Lu, T. *et al.* Probing ion permeation and gating in a K^+ channel with backbone mutations in the selectivity filter. *Nat. Neurosci.* **4**, 239–246 (2001).
22. Alagem, N., Yesylevskyy, S. & Reuveny, E. The pore helix is involved in stabilizing the open state of inwardly rectifying K^+ channels. *Biophys. J.* **85**, 300–312 (2003).
23. Chapman, M.L., VanDongen, H.M. & VanDongen, A.M. Activation-dependent subconductance levels in the drk1 K channel suggest a subunit basis for ion permeation and gating. *Biophys. J.* **72**, 708–719 (1997).
24. Proks, P., Capener, C.E., Jones, P. & Ashcroft, F.M. Mutations within the P-loop of Kir6.2 modulate the intraburst kinetics of the ATP-sensitive potassium channel. *J. Gen. Physiol.* **118**, 341–353 (2001).
25. Zheng, J. & Sigworth, F.J. Selectivity changes during activation of mutant Shaker potassium channels. *J. Gen. Physiol.* **110**, 101–117 (1997).
26. Hoshi, T., Zagotta, W.N. & Aldrich, R.W. Two types of inactivation in Shaker K^+ channels: effects of alterations in the carboxy-terminal region. *Neuron* **7**, 547–556 (1991).
27. Kiss, L., LoTurco, J. & Korn, S.J. Contribution of the selectivity filter to inactivation in potassium channels. *Biophys. J.* **76**, 253–263 (1999).
28. Liu, Y., Jurman, M.E. & Yellen, G. Dynamic rearrangement of the outer mouth of a K^+ channel during gating. *Neuron* **16**, 859–867 (1996).
29. Lopez-Barneo, J., Hoshi, T., Heinemann, S.H. & Aldrich, R.W. Effects of external cations and mutations in the pore region on C-type inactivation of Shaker potassium channels. *Receptors Channels* **1**, 61–71 (1993).
30. Lu, Z., Klem, A.M. & Ramu, Y. Ion conduction pore is conserved among potassium channels. *Nature* **413**, 809–813 (2001).
31. Gao, L., Mi, X., Paajanen, V., Wang, K. & Fan, Z. Activation-coupled inactivation in the bacterial potassium channel KcsA. *Proc. Natl. Acad. Sci. USA* **102**, 17630–17635 (2005).
32. Zhou, Y., Morais-Cabral, J.H., Kaufman, A. & MacKinnon, R. Chemistry of ion coordination and hydration revealed by a K^+ channel-Fab complex at 2.0 A resolution. *Nature* **414**, 43–48 (2001).
33. Kuo, A. *et al.* Crystal structure of the potassium channel KirBac1.1 in the closed state. *Science* **300**, 1922–1926 (2003).
34. Yang, J., Yu, M., Jan, Y.N. & Jan, L.Y. Stabilization of ion selectivity filter by pore loop ion pairs in an inwardly rectifying potassium channel. *Proc. Natl. Acad. Sci. USA* **94**, 1568–1572 (1997).
35. Choi, H. & Heginbotham, L. Functional influence of the pore helix glutamate in the KcsA K^+ channel. *Biophys. J.* **86**, 2137–2144 (2004).
36. Ficker, E., Jarolimek, W., Kiehn, J., Baumann, A. & Brown, A.M. Molecular determinants of dofetilide block of HERG K+ channels. *Circ. Res.* **82**, 386–395 (1998).
37. Kuriyan, J., Petsko, G.A., Levy, R.M. & Karplus, M. Effect of anisotropy and anharmonicity on protein crystallographic refinement. An evaluation by molecular dynamics. *J. Mol. Biol.* **190**, 227–254 (1986).
38. Doyle, D.A. *et al.* The structure of the potassium channel: molecular basis of K^+ conduction and selectivity. *Science* **280**, 69–77 (1998).
39. Berneche, S. & Roux, B. Energetics of ion conduction through the K+ channel. *Nature* **414**, 73–77 (2001).
40. Zhou, Y. & MacKinnon, R. The occupancy of ions in the K^+ selectivity filter: charge balance and coupling of ion binding to a protein conformational change underlie high conduction rates. *J. Mol. Biol.* **333**, 965–975 (2003).
41. Lenaeus, M.J., Vamvouka, M., Focia, P.J. & Gross, A. Structural basis of TEA blockade in a model potassium channel. *Nat. Struct. Mol. Biol.* **12**, 454–459 (2005).
42. Delcour, A.H., Martinac, B., Adler, J. & Kung, C. Modified reconstitution method used in patch-clamp studies of *Escherichia coli* ion channels. *Biophys. J.* **56**, 631–636 (1989).
43. Cortes, D.M. & Perozo, E. Structural dynamics of the *Streptomyces lividans* K^+ channel (SKC1): oligomeric stoichiometry and stability. *Biochemistry* **36**, 10343–10352 (1997).
44. Cortes, D.M., Cuello, L.G. & Perozo, E. Molecular architecture of full-length KcsA: role of cytoplasmic domains in ion permeation and activation gating. *J. Gen. Physiol.* **117**, 165–180 (2001).
45. Otwinowski, Z. & Minor, W. Processing of X-ray diffraction data collected in oscillation mode. *Methods Enzymol.* **276**, 307–326 (1997).
46. Jones, T.A., Zou, J.-Y., Cowans, S.W. & Kjeldgaard, M. Improved methods for building protein models in electron-density maps and the location of errors in these models. *Acta Crystallogr. A* **47**, 110–119 (1991).
47. Brunger, A.T. *et al.* Crystallography and NMR system: a new software suite for macromolecular structure determination. *Acta Crystallogr. D Biol. Crystallogr.* **54**, 905–921 (1998).
48. Berneche, S. & Roux, B. Molecular dynamics of the KcsA K^+ channel in a bilayer membrane. *Biophys. J.* **78**, 2900–2917 (2000).
49. Woo, H.J., Dinner, A.R. & Roux, B. Grand canonical Monte Carlo simulations of water in protein environments. *J. Chem. Phys.* **121**, 6392–6400 (2004).
50. Pettersen, E.F. *et al.* Chimera—a visualization system for exploratory research and analysis. *J. Comput. Chem.* **25**, 1605–1612 (2004).